Check for updates

Nanoparticle-assisted structural tailoring of trehalose lipid biosynthesis by *Rhodococcus erythropolis* WJ-2

Yifei Meng,[†a] Xuan Ou,[†a] Zhenghui Liu,[†b] Shun Yao,[a] Chuxiao Hu,[a] Qiuchi Yu[c] and Wenjie Xia [ID] [†*a]

Achieving sustainable and cost-effective production and modulating the structure of biosurfactants is increasingly obtaining attention due to carbon neutrality and eco-safety. Nanotechnology-assisted approaches have been emerging as a promising strategy for this purpose. Here, we investigated the effect of metal oxide nanoparticles on the yield and molecular structure of trehalose lipids produced by *Rhodococcus erythropolis* WJ-2. Sunflower oil was identified as the optimal carbon source against other oils, yielding 12.60 g L^{-1}. Subsequent optimization of four key medium components (sunflower oil, $ZnSO_4$, $(NH_4)_2SO_4$, and yeast extract) using a Box–Behnken design elevated the baseline yield to 24.75 g L^{-1}. Interestingly, the trehalose lipid yield was further enhanced to 28.12 g L^{-1} compared to the optimized medium without NPs when supplemented with 0.5 g per L Fe_2O_3 NPs ($\approx$20 nm). Furthermore, structural diversity analyzed by FTIR and HPLC-MS showed the obvious *m/z* value shifts of trehalose lipids with NPs comprising longer hydrophobic fatty acid chains and more unsaturated fatty acid derivatives. In the absence of Fe_2O_3 NPs, the main *m/z* peaks were detected at *m/z* 496, 694, 877, and 1044 (relative abundances: 14.19%, 27.08%, 44.18%, 14.55%), corresponding to short-to-medium-chain fatty acid derivatives (*e.g.*, methyl hexanoate, methyl octanoate). In contrast, the dominant peaks shifted to *m/z* 673, 807, 874, and 1043 (relative abundances: 22.21%, 18.39%, 47.64%, 11.76%) with Fe_2O_3 NP supplementation. These findings suggest that the unique redox properties and high surface area of Fe_2O_3 nanoparticles could enhance the yield and modulate the structures to enable the tailored biosynthesis of glycolipids by influencing key-enzyme activity and metabolic flux. This nanoparticle-assisted fermentation strategy offers a promising route for the scalable production of designer biosurfactants for diverse industrial applications.

1. Introduction

Microbial biosurfactants have increasingly emerged as sustainable alternatives to synthetic surfactants due to their biodegradability, low toxicity, and robust performance under extreme conditions.[1,2] Their capacity to reduce surface and interfacial tensions renders them indispensable for applications such as enhanced oil recovery, environmental remediation, and pharmaceutical formulations.[3–5] The global biosurfactant market is also expanding rapidly, and it is expected that the market revenue will reach more than 6-billions

dollars by 2030.[6,7] However, the widespread commercialization of these products is severely hindered by their excessively high production costs. The main reasons are the unsatisfactory fermentation yields and the complex downstream processing procedures.[8] Extensive research has demonstrated that the optimization of fermentation parameters and the refinement of downstream processing techniques can substantially enhance production efficiency while reducing overall manufacturing costs.[9]

Among the diverse classes of biosurfactants, glycolipids have attracted significant attention owing to their unique molecular architectures. In particular, trehalose lipids are characterized by having a hydrophilic trehalose moiety that is linked to one or more hydrophobic fatty acid chains. This configuration produces a spectrum of molecules that vary in fatty acid chain length, degree of saturation, and glycosidic linkage, all of which critically influence key performance parameters such as the critical micelle concentration (CMC), emulsification efficiency, and interfacial tension.[10,11] Comprehensive understanding of the structure–function relationship of trehalose lipids is

[a]Key Laboratory of Molecular Microbiology and Technology, Ministry of Education, College of Life Sciences, Nankai University, Tianjin, P. R. China. E-mail: wenjie. xia@nankai.edu.cn

[b]Tianjin Academy of Agricultural Sciences, Huada Road, 17th Kilometric Marker of Jinjing Highway, Xiqing District, Tianjin 300381, China

[c]Technical Management Office, Ninth Oil Production Plant, Daqing Oilfield Co., Ltd, Longhupao Oil Production Operation Area, China

† These authors equally contributed to this study.

foundational to tailoring their properties *via* biosynthetic engineering—specifically, by manipulating the expression of key enzymes involved in trehalose synthesis (*e.g.*, trehalose-6-phosphate synthase/phosphatase) and fatty acid chain elongation/acylation (*e.g.*, acyltransferases). In depth understanding of the structure–function relationship of biosurfactants can be used to adjust the properties of biosurfactants, which is crucial for meeting specific industrial needs and reducing the required effective dosage, thereby reducing production costs.[12,13]

Trehalose lipids play significant roles in multiple fields. As biosurfactants, they can disrupt bacterial cell walls and exhibit notable antimicrobial activity. The underlying mechanism may involve fatty acids damaging microbial cell structures, leading to cytoplasmic leakage, or interfering with respiratory chain electron transport systems associated with biofilms. Studies have shown that trehalose lipids at a concentration of $300\ mg\ L^{-1}$ can inhibit the germination of filamentous fungal conidia.[14] The antimicrobial properties of trehalose lipids make them suitable for use as food preservatives. For instance, Zhang Qing *et al.*[15] developed a novel food preservative primarily composed of trehalose monofumarate (TMF), which demonstrates strong antibacterial and antifungal activities. TMF exhibits a broad antimicrobial spectrum, effectively inhibiting the growth of common microorganisms such as *Escherichia coli*, *Bacillus subtilis* and *Saccharomyces cerevisiae*. Biosurfactants like trehalose lipids enhance the solubility of organic compounds, promoting the dispersion, solubilization, and emulsification of pollutants to accelerate their degradation. They also reduce the interfacial tension between crude oil and water, thereby improving oil recovery efficiency in petroleum extraction. Although glycolipid biosurfactants possess unparalleled advantages over other surfactants, these benefits alone are insufficient to support large-scale production. Therefore, while advancing fundamental research, it is essential to consider the potential commercial value and economic benefits of trehalose lipids. Only by addressing these challenges can trehalose lipid-based products meet market expectations and become efficient, cost-effective, and environmentally friendly biosurfactants.

Rhodococcus erythropolis has emerged as a promising candidate for trehalose lipid production due to its versatile metabolic capabilities and its ability to utilize a wide range of hydrophobic substrates, including vegetable oils and hydrocarbons.[16,17] Some studies have further demonstrated that *Rhodococcus erythropolis* can utilize organic wastes (such as cooking oil) as substrates, which not only reduces production costs but also enhances environmental sustainability.[18] Traditional strategies for enhancing the production of biosurfactants mainly focus on adjusting the carbon and nitrogen sources, as well as adding soluble metal ions (*e.g.*, Fe^{2+}, Zn^{2+}, Mn^{2+}) to the culture medium, which serve as cofactors for key enzymes in lipid biosynthesis.[6,7] While these strategies have led to modest enhancements in fermentation performance, their ability to influence the molecular structure, as a result, the functional properties of trehalose lipids remain inherently constrained.[3] In recent years, synthetic biology and metabolic engineering have revolutionized microbial cell factory design, offering precise

tools to rewire biosynthetic pathways for trehalose lipid production. Strategies for engineering microbial cell factories have been developed at various levels, ranging from molecular and pathway engineering to genome-scale modifications[19,20] and enable precise control over the expression levels of key enzymes involved in biosurfactant synthesis[21] for the enhanced production. These strategies span from targeted gene overexpression/knockdown to genome-scale metabolic modeling (GSMM) and pathway flux optimization, enabling fine-tuned control over the expression of rate-limiting enzymes in trehalose lipid biosynthesis. However, genetic engineering approaches still face challenges, including unstable heterologous gene expression, biosafety concerns associated with genetically modified organisms (GMOs), and economic/regulatory barriers to large-scale commercialization—limitations that motivate the exploration of complementary biotechnological tools.

In recent years, the application of metal oxide nanoparticles has emerged as a promising approach to replace traditional soluble metal ion supplements. Owing to their high surface area-to-volume ratios and unique redox properties, nanometal oxides can enhance enzymatic activity, facilitate electron transfer, and provide localized, sustained metal ion release—mechanisms that differ substantially from those of soluble ions.[12,22] For example, studies in rhamnolipid and sophorolipid systems have demonstrated that nanoparticle supplementation can not only elevate biosurfactant yields but also induce modifications in molecular structure, such as alterations in fatty acid chain length, degree of saturation, and glycosidic bond configuration.[1,3] These structural changes are associated with the enhancement of emulsifying properties and the decrease of the critical micelle concentration (CMC), thus reducing the dosage required for effective performance and contributing to the reduction of the overall production cost.[8,11] Moreover, the antimicrobial properties of nanoparticles offer new possibilities for the application of biosurfactants in the pharmaceutical field.[23,24] The design and application of functional nanomaterials have emerged as a cutting-edge frontier in biomedical research. For example, curcumin-based polymer-gold nanocomposites (C-PVP-Au) have been demonstrated to effectively inhibit amyloid protein aggregation, disrupt bacterial cell membranes, and promote wound healing.[25] These capabilities are largely attributed to their enhanced bioavailability, stability, and unique capacity to interact with biomolecules and cellular structures. These properties suggest that such nanoparticles may not only serve as efficient drug delivery vehicles, but also represent potential tools for regulating complex cellular metabolic processes. Of particular relevance is lipid biosynthesis—a central pathway involved in cellular energy homeostasis, membrane architecture, and signal transduction, whose dysregulation is closely linked to various pathological conditions, including metabolic syndrome.

Iron oxide nanoparticles were selected for this study primarily because iron serves as an essential cofactor for key enzymes involved in trehalose lipid biosynthesis, including fatty acid synthases, acyltransferases, and cytochrome P450 enzymes, which directly participate in fatty acid chain

elongation, trehalose acylation, and redox reactions. The nanoparticles enable controlled release of iron ions, thereby avoiding the cytotoxicity associated with soluble iron surges and ensuring sustained enzymatic support. Moreover, the inherent redox properties of iron oxide facilitate microbial electron transfer and enhance NADPH dependent lipid synthesis, effectively channeling metabolic flux toward the targeted product, in contrast to the passive carrier function of inert materials. Despite these encouraging findings in related biosurfactant systems, the effect of nanoparticle supplementation on trehalose lipid production by *R. erythropolis* remains relatively underexplored. Therefore, this study systematically investigates the influence of iron oxide nanoparticles (Fe$_2$O$_3$) on both the fermentation performance and molecular structure of trehalose lipids produced by *R. erythropolis* WJ-2. By integrating kinetic growth analyses, fermentation yield assessments, and Fourier Transform Infrared (FTIR) spectroscopy for structural characterization, we demonstrate that moderate Fe$_2$O$_3$ supplementation (0.5 g L^{-1}) enhances trehalose lipid production by approximately 10% relative to control conditions. Furthermore, our FTIR data reveal subtle yet significant shifts in spectral features, which indicate of modifications in fatty acid chain length, saturation, or glycosidic linkages. These findings underscore the potential of nanoparticle-assisted fermentation to tailor the functional properties of biosurfactants.[4,10] Compared to traditional soluble metal ions, the localized release characteristics of nanoparticles enable more precise regulation of microbial metabolism, thereby enhancing the yield and quality of target products.[26] By comparing our findings with those from other biosurfactant systems, we illustrate that nanoparticle-assisted fermentation offers a promising route to simultaneously improve production yields and modulate the molecular characteristics of trehalose lipids, thereby advancing the commercial viability of these versatile bioproducts. Future studies should focus on integrating nanoparticles with advanced biotechnological approaches, including metabolic engineering and synthetic biology,[27] to optimize biosurfactant production processes, thereby enhancing both efficiency and cost-effectiveness.

2. Materials and methods

2.1. Strain and culture

The *Rhodococcus erythropolis* WJ-2 strain was obtained from our laboratory's culture collection (City/Institution, Country) and stored in 25% (v/v) glycerol at −80 °C. This strain has previously been reported to synthesize trehalose lipids with promising biosurfactant properties. All chemicals and reagents, including yeast extract, tryptone, agar, NaCl, Na$_2$HPO$_4$, KH$_2$PO$_4$, MgSO$_4$, ZnSO$_4$, (NH$_4$)$_2$SO$_4$, CaCl$_2$, FeSO$_4$, MnSO$_4$, ethyl acetate, and HCl, were of analytical grade (Sigma-Aldrich, St. Louis, MO, USA, unless otherwise specified). Corn syrup dry powder (food-grade) was purchased from a local supplier. Deionized water (18.2 MΩ cm at 25 °C; Millipore Corp., Burlington, MA, USA) was used for all media preparations.

Sunflower oil, peanut oil, isododecane, and isohexadecane (all ≥99% purity) were procured from Aladdin (Shanghai,

China). Iron oxide nanoparticles (Fe$_2$O$_3$, ∼20 nm) were obtained from Sigma-Aldrich. The basic medium for fermentation composed of (per liter): 2.5 g Na$_2$HPO$_4$, 1.0 g KH$_2$PO$_4$, 2.5 g (NH$_4$)$_2$SO$_4$, 0.5 g MgSO$_4$, 0.1 g ZnSO$_4$, 0.05 g CaCl$_2$, 1.0 g yeast extract, 1.0 g corn syrup dry powder, and 15% (v/v) hydrophobic carbon source (unless otherwise specified). FeSO$_4$ (0.1 g L^{-1}) and MnSO$_4$ (0.01 g L^{-1}) were filter-sterilized (0.22 μm) and added aseptically post-autoclaving. pH adjusted to 7.0 ± 0.2 prior to sterilization at 121 °C for 20 min. All media were prepared with deionized water and stored at 4 °C when not in use. Unless otherwise specified, aerobic batch cultures were grown in 250 mL Erlenmeyer flasks containing 100 mL of medium, shaken at 200 rpm, and maintained at 37 °C.

Bacterial growth was tracked *via* colony-forming unit enumeration. Specifically, 1 mL culture samples were serially diluted (tenfold) in sterile phosphate-buffered saline (PBS, pH 7.2). From each dilution, 100 μL was plated in triplicate on LB agar. After 24 h of incubation at 37 °C, colony counts were recorded, and cfu mL^{-1} was calculated. Growth curves (log cfu mL^{-1} *vs.* time) revealed the lag, exponential, and stationary growth phases.

2.2. Trehalose lipid quantification

The harvested broth was autoclaved at 121 °C for 20 min and then acidified to pH ∼3.0 with 1 M HCl, aiding in the separation of microbial biomass and extracellular products.[10] After centrifugation at 10 000 rpm for 10 min, the supernatant and the intermediate layer were transferred into a separatory funnel and extracted with an equal volume of ethyl acetate (≥99.5% purity). Typically, three successive extractions were performed. The combined organic layers were concentrated under reduced pressure at 40–45 °C in a rotary evaporator. The resulting semi-transparent, yellowish material, designated as "crude trehalose lipid", was dried to constant weight. Crude yields (g L^{-1}) were computed by dividing the mass of the dried product by the initial culture volume.[14]

2.3. Production optimization

To identify the optimal hydrophobic substrate for trehalose lipid production, peanut oil, sunflower oil, isododecane, and isohexadecane were individually tested in the fermentation medium described in Section 2.1, each at 15% (v/v). The seed culture (10% inoculum, v/v) was transferred into 100 mL of each test medium, followed by incubation at 37 °C and 200 rpm for up to 7 days.[13] Culture aliquots (1 mL) were taken every 24 h to assess cell growth (Section 2.2) and trehalose lipid yields (Section 2.2).

2.3.1. Effect of iron oxide nanoparticles on trehalose lipid production. To investigate whether iron oxide nanoparticles (Fe$_2$O$_3$) could further enhance trehalose lipid output, four concentrations (0, 0.1, 0.5, and 1.0 g L^{-1}) were tested under the optimized medium conditions established *via* the Box–Behnken design. Cultures were prepared in triplicate, inoculated at 10% (v/v), and incubated for 7 days.[20] Samples were taken every 24 h to monitor cell growth (cfu mL^{-1}) and final trehalose lipid yields (g L^{-1}).

2.3.2. Optimization of trehalose lipid production using a Box–Behnken design. A Box–Behnken design (Design-Expert 13, Stat-Ease Inc., MN, USA) was employed to optimize four variables in the fermentation medium for trehalose lipid production: (i) sunflower oil (A), (ii) $ZnSO_4$ (B), (iii) $(NH_4)_2SO_4$ (C), and (iv) yeast extract (D).[2] Each factor was tested at three coded levels (−1, 0, +1), and trehalose lipid yield (g L^{-1}) served as the response variable. The experiments were carried out in randomized order to minimize bias. Following incubation (Section 2.2), each culture was extracted as in Section 2.2, and the crude product yield was recorded. In order to analyze the data, a quadratic polynomial model was adopted, and the significance of the linear effects, quadratic effects, and inter-action effects was evaluated through analysis of variance (ANOVA).

2.4. FTIR spectroscopy

The crude trehalose lipid extracts were detected by Fourier transform infrared spectroscopy (FTIR) using a Nicolet iS50 spectrometer (Thermo Fisher Scientific, USA). Approximately 5–10 mg of the vacuum-dried sample was mixed with spectroscopic-grade potassium bromide (KBr) and pressed into pellets. Spectra were collected from 4000 to 400 cm^{-1} at a resolution of 4 cm^{-1}. Key absorption bands, particularly the O–H stretch ($\sim$3400 cm^{-1}), the aliphatic C–H stretch ($\sim$2900 cm^{-1}), and sugar ring vibrations (900–1000 cm^{-1}), to confirm the presence of trehalose-based glycolipids.[10,20]

2.5. HPLC-MS identification

Crude trehalose lipid extracts were prepared as described previously and reconstituted in HPLC-grade methanol (1 mg mL^{-1}). The solution was filtered through a 0.22 μm PTFE filter prior to analysis. HPLC-MS analysis followed the reported method.[1,10]

Chromatographic separation was conducted on a reversed-phase C18 column (2.1 × 100 mm, 1.7 μm) maintained at 40 °C. The mobile phase comprised 0.1% formic acid in water (Solvent A) and 0.1% formic acid in acetonitrile (Solvent B). A gradient elution was employed: 30% B for 2 min, a linear increase to 100% B over 30 min, a 5-min hold at 100% B, followed by a 5-min re-equilibration at 30% B. The flow rate was set at 0.3 mL min^{-1} with a 5 μL injection volume. Mass spectrometric detection was performed on a high-resolution QTOF instrument (*e.g.*, Waters Xevo G2-XS) equipped with an electrospray ionization (ESI) source operated in both positive and negative ion modes. Key parameters were: capillary voltage 3.0 kV, cone voltage 40 V, desolvation temperature 350 °C, and desolvation gas flow 800 L h^{-1}. Full-scan spectra were obtained within the m/z range of 200–2000, and data-dependent MS/MS acquisition was employed for structural elucidation.

2.6. Statistical analyses

All experiments were carried out at least in duplicate ($n \geq 2$), and results are presented as mean ± standard deviation. Statistical analyses were performed with SPSS (IBM, Armonk, NY, USA) and the built-in modules of Design-Expert 13.[6] ANOVA was used to evaluate the significance of regression models, with $p < 0.05$ considered statistically significant. Figures illustrating growth curves, trehalose lipid yields, and response surface plots were prepared using OriginPro 9.1 (OriginLab, Northampton, MA, USA).

2.7. Scanning electron microscopy of *Rhodococcus erythropolis* WJ-2 and Fe_2O_3 nanoparticles

Resuspend 20 μm Fe_2O_3 nanoparticles (0.5 g L^{-1}) in deionized water and treat with an ultrasonic cleaner for 30 min to ensure uniform dispersion of the particles. Mix the bacteria in the logarithmic growth phase with an equal volume of the ultra-sonically treated nanoparticles and co-incubate. Collect the precipitate by centrifugation and wash it repeatedly with PBS buffer. Then fix it with 2.5% glutaraldehyde, dehydrate it using ethanol in different gradients, and finally perform freeze-drying. Observe the treated complex using a scanning electron microscope (QUANTA 200, FEI Company America).

3. Results and discussion

3.1. Colony characteristics

Morphological observations showed that *Rhodococcus erythropolis* WJ-2 formed beige to orange colonies on LB agar, with a diameter of approximately 1–2 millimeters. Under microscopic examination, the edges were slightly translucent, and no significant pigment diffusion into the medium was observed (Figure1).This morphological profile is consistent with earlier reports on *Rhodococcus* species, which commonly exhibit distinctive pigmentation and relatively slow growth on solid media.[14] Based on the 16S rRNA gene sequence, a phylogenetic tree was constructed to illustrate the relationship between strain WJ-2 and other closely related *Rhodococcus* species. Sequence analysis revealed that WJ-2 exhibits over 99% similarity to known *Rhodococcus* strains. The uniform colony characteristics and stable coloration observed here suggest that WJ-2 may be highly suitable for industrial fermentation processes, as consistent colony morphology is generally associated with genetic stability of *Rhodococcus* strains.[15]

3.2. Effect of carbon sources on trehalose lipid production

3.2.1. Cell growth. Four hydrophobic substrates—peanut oil, sunflower oil, isododecane, and isohexadecane, which were individually evaluated to assess their influence on *R. erythropolis* WJ-2 growth (Fig. 2). Although all cultures displayed a characteristic sigmoidal growth pattern, the timing of peak cell densities and the magnitude of viable counts varied substantially.

The growth profiles of *Rhodococcus* sp. varied significantly depending on the carbon source provided. Peanut oil supported robust growth, with biomass accumulation increasing steadily between 24 and 96 h. This observation aligns with previous studies demonstrating that oil-based substrates can promote high biomass yields in *Rhodococcus* species.[2] In contrast, sunflower oil induced a rapid increase in cell numbers,
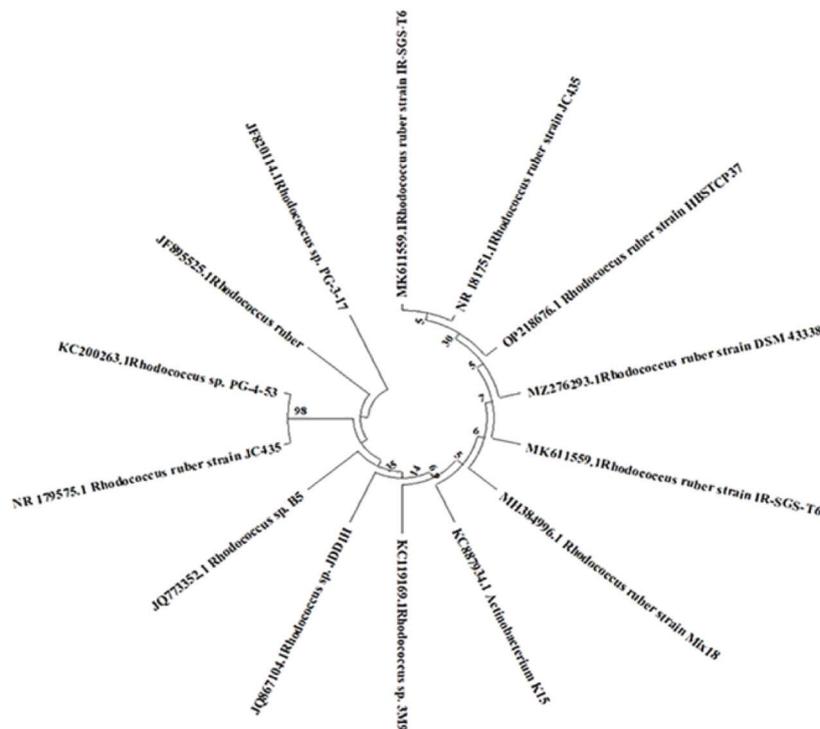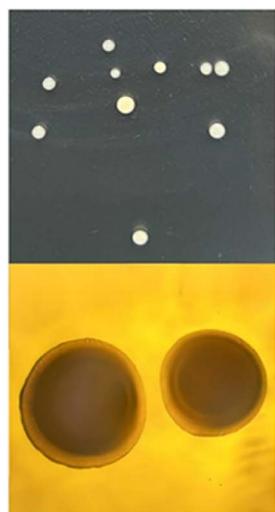
Fig. 1 Colony morphology of *Rhodococcus erythropolis* WJ-2 and phylogenetic tree analysis of *Rhodococcus* sp. WJ-2.

reaching a peak at approximately 48 h, after which a decline in cell viability was observed. Isododecane, however, exhibited a more gradual growth pattern, with maximum cell density achieved around 72 h. Notably, isohexadecane resulted in delayed growth kinetics and the lowest overall cell density, suggesting limited utilization of this substrate by the strain.[22]
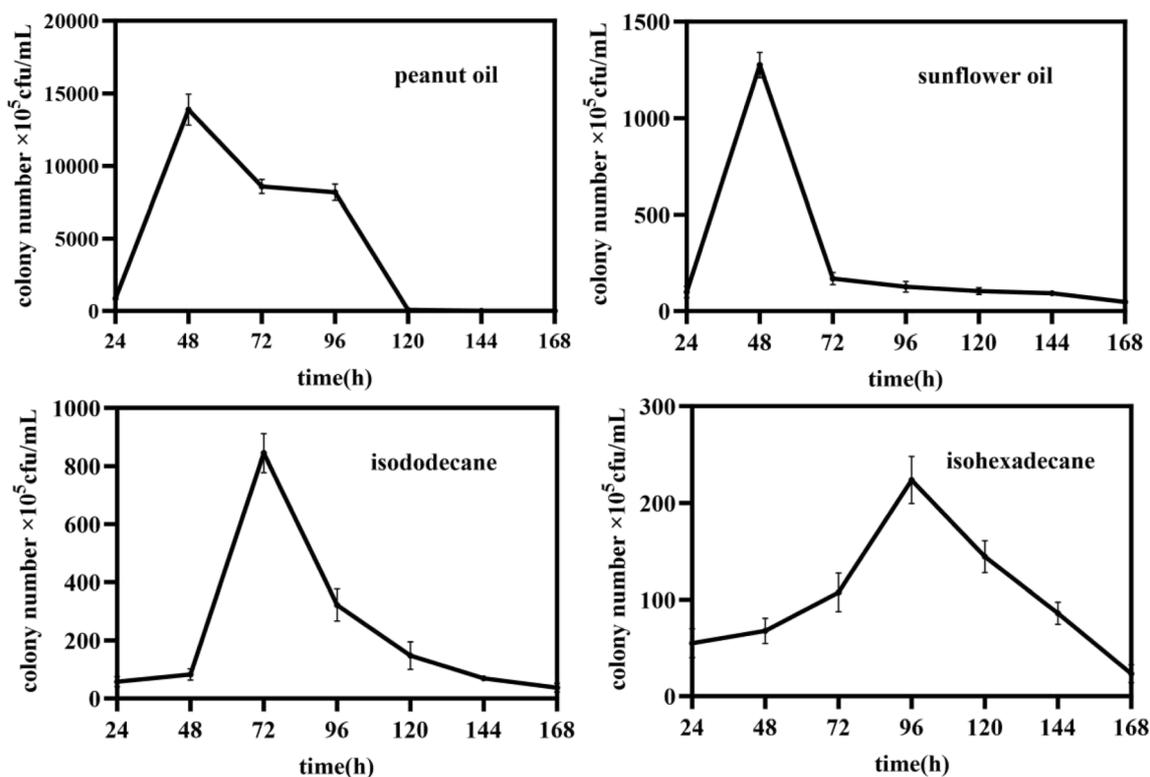

Fig. 2 Growth curves of strains under different carbon sources.

© 2026 The Author(s). Published by the Royal Society of Chemistry
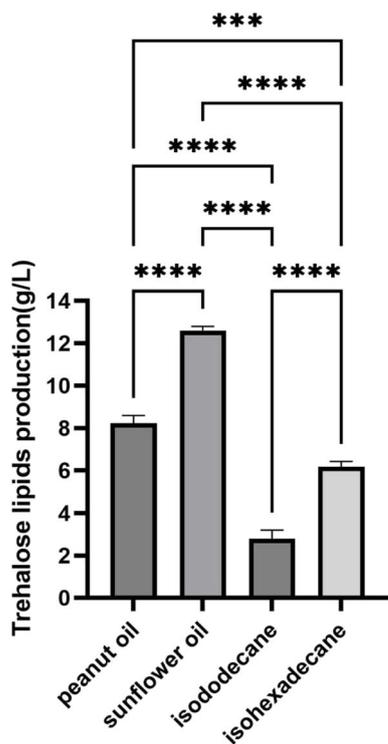
Fig. 3 Trehalose lipids production under different carbon sources.

By approximately 144 h, all cultures converged to comparatively low cell densities, suggesting that nutrient depletion or accumulation of inhibitory metabolites may have curtailed further microbial proliferation.[7] This observation indicates that 144 h is a crucial time point for harvesting the fermentation broth, which can strike a balance between high cell density and product accumulation.

3.2.2. Trehalose lipid yield across carbon sources. Trehalose lipid yields (Fig. 3) revealed a clear advantage for sunflower oil: cultures grown on sunflower oil reached 12.60 g L^{-1}, notably surpassing the other tested substrates. This result is consistent with previous studies, indicating that the fatty acid composition of sunflower oil contributes to the biotransformation by microorganisms, thereby increasing the yield of biosurfactants.[1] Although peanut oil also sustained significant cell growth, its overall trehalose lipid yield was slightly lower than sunflower oil's under the tested conditions, indicating that not all vegetable oils are equally efficient for glycolipid production.[2] Meanwhile, isododecane and isohexadecane

Table 1 Box–Behnken experimental design

Factors	Coding level		
	−1	0	1
Sunflower oil %	10	15	20
$(NH_4)_2SO_4$ g L^{-1}	2	2.5	3
$ZnSO_4$ g L^{-1}	0	0.1	0.2
Yeast extract g L^{-1}	0.5	1	1.5

supported lower yields, likely due to lower bioavailability and the limited enzymatic repertoire of WJ-2 for breaking down branched or long-chain hydrocarbons.[16]

Collectively, these findings underscore the importance of substrate selection for trehalose lipid biosynthesis. Sunflower oil emerged as a promising candidate for large-scale processes, warranting additional medium optimization.

3.3. Optimization of fermentation medium *via* Box–Behnken design

3.3.1. Experimental setup and observations. A Box–Behnken design was employed to refine four key medium components—sunflower oil (A), $ZnSO_4$ (B), $(NH_4)_2SO_4$ (C), and yeast extract (D), based on the initial evidence that sunflower oil is the most effective carbon source. Table 1 summarizes the design matrix, while figure (SI) illustrates the cell growth trends for each run. Although most runs exhibited a notable decline in cell counts after 72 h, trehalose lipid titers displayed wide variability (13–22 g L^{-1}), highlighting the complex interactions among carbon, nitrogen, and trace metal supplementation.[10]

This result aligns with multiple past reports demonstrating that microbial glycolipid production depends not only on the primary carbon source but also on balanced macronutrient and micronutrient availability.[6] In particular, *Rhodococcus* species often require specific concentrations of metal ions (*e.g.*, Zn^{2+}, Fe^{2+}/Fe^{3+}) for the functioning of membrane-bound oxygenases that participate in lipid catabolism.

3.3.2. Quadratic regression modeling and ANOVA. According to the results of the analysis of variance (ANOVA), the fitted second-order polynomial model was statistically significant ($P < 0.05$), and the adjusted R^2 value was higher than 0.99 (Table 2). This high coefficient of determination indicates that the variation in the yield of trehalose lipids is mainly determined by the selected factors. In addition, the model also revealed significant interactions, especially the interaction between sunflower oil (A) and $(NH_4)_2SO_4$ (C), which suggests that the supply of the nitrogen source can affect the metabolic efficiency of the strain towards hydrophobic substrates.[7]

Response surface plots (SI) corroborated these interactions: excessive or insufficient concentrations of trace metals and nitrogen sources hindered trehalose lipid synthesis, whereas a balanced milieu enhanced both cell density and extracellular glycolipid excretion. Numerical optimization pinpointed sunflower oil at around 16.4% (v/v), $(NH_4)_2SO_4$ at 2.0 g L^{-1}, $ZnSO_4$ at 0.17 g L^{-1}, and yeast extract at 1.5 g L^{-1} as optimal. Validation experiments under these conditions yielded an average trehalose lipid concentration of 24.75 g L^{-1}, closely matching the model's prediction. This represents an increase of 11.24% compared to the level before optimization, highlighting the crucial role played by the statistical design approach in the research of microbial biosurfactants.[16,22]

3.4. Effect of iron oxide nanoparticles on trehalose lipid production

3.4.1. Impact on cell growth. Encouraged by recent findings that metal oxide nanoparticles can stimulate microbial

Table 2 Regression model analysis of variance

Source	DF	SS	MS	F-value	p-value
A–A	1	4.05	4.05	129.48	0.0558
B–B	1	0.2400	0.2400	7.68	0.2205
C–C	1	5.38	5.38	172.04	0.0484*
D–D	1	2.16	2.16	69.12	0.0762
AB	1	4.76	4.76	152.38	0.0515
AC	1	15.43	15.43	493.92	0.0286*
AD	1	1.39	1.39	44.52	0.0947
BC	1	0.9339	0.9339	29.88	0.1152
BD	1	36.91	36.91	1180.98	0.0185*
CD	0	0.0000			
A^2	1	18.98	18.98	607.29	0.0258*
B^2	0	0.0000			
C^2	0	0.0000			
D^2	0	0.0000			
Model	10	87.34	8.73	279.47	0.0465*
Pure error	1	0.0313	0.0313		
Cor total	11	87.37			

metabolism, iron oxide nanoparticles were incorporated at concentrations of 0, 0.1, 0.5, and 1.0 g L^{-1}. The growth curves (Fig. 4) showed that 0.5 g per L Fe_2O_3 sustained the highest viable cell counts, particularly during the mid-exponential phase (24–48 h). In addition, although the initial concentration of 1.0 g L^{-1} could support the rapid growth of cells, it significantly decreased after 48 hours. It is speculated that this may be related to the cytotoxicity generated at a higher concentration of nanoparticles or the particle aggregation effect.[22]

3.4.2. Enhancement of trehalose lipid yield. Under the optimized fermentation conditions (16.4% sunflower oil, 2.0 g per L $(NH_4)_2SO_4$, 0.17 g per L $ZnSO_4$, 1.5 g per L yeast extract), trehalose lipid production reached ~24.75 g L^{-1} in the absence of nanoparticles, closely matching the model's forecast of 24.63 g L^{-1} (Fig. 5). Notably, supplementation with 0.5 g per L Fe_2O_3 increased yields to 28.12 g L^{-1}, suggesting a positive role of iron oxide nanoparticles in enhancing metabolic fluxes or stabilizing relevant enzymes.[7] By contrast, 0.1 g L^{-1} had negligible effect, and 1.0 g L^{-1} exerted an inhibitory effect on final lipid accumulation.
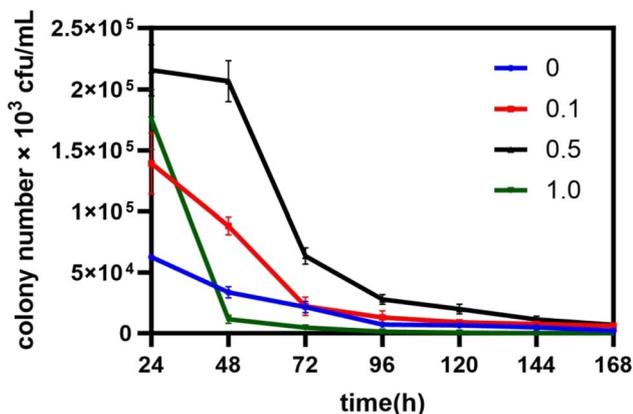

Fig. 4 Growth curves of strains with different iron oxide nanoparticles.
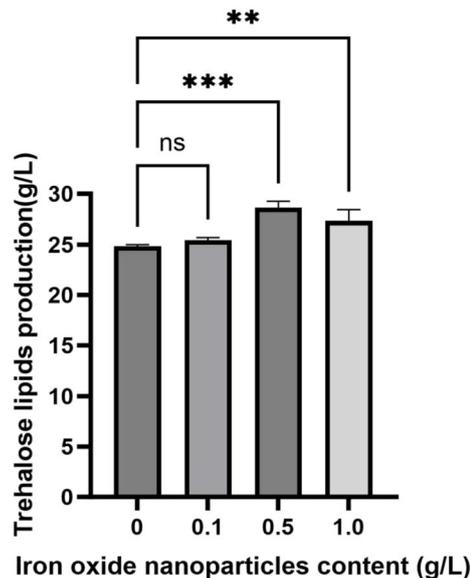

Fig. 5 Trehalose lipids production at different iron oxide nanoparticles content.

These results are consistent with emerging perspectives in nanoparticle–microbe interactions, wherein moderate nanoparticle concentrations can improve electron transport chain efficiency or enzyme cofactors, thereby boosting the production of secondary metabolites.[6] However, a high concentration of nanoparticles may disrupt the cell membrane structure or trigger oxidative stress, thus offsetting the potential advantages of biosurfactant synthesis.[2] Through further biochemical and transcriptomic analyses, the specific mechanism by which 0.5 g L^{-1} of Fe_2O_3 exerts a stimulatory effect on *Rhodococcus* sp. WJ-2 can be more deeply elucidated.

3.5. FTIR spectroscopy analysis

The Fourier transform infrared spectroscopy (FTIR) of the crude trehalose lipids (Fig. 6) showed multiple characteristic absorption peaks: ~3420 cm^{-1} the O–H stretching vibration peak, indicating the presence of hydroxyl groups in trehalose; ~2950–2860 cm^{-1}: aliphatic C–H stretching, associated with the lipid moieties; ~1650 cm^{-1}: weak carbonyl (C=O) signal, suggesting minor ester or keto groups; ~1200–1450 cm^{-1}: C–O vibrations indicative of fatty acid ester linkages; 900–1000 cm^{-1}: sugar ring vibrations, confirming the presence of a glycosidic structure.

These features align with known profiles of trehalose-containing glycolipids produced by *Rhodococcus* spp. and reaffirm the successful production and isolation of trehalose lipids in this study.[10] The strong signals observed in the aliphatic region (2950–2860 cm^{-1}) indicate the presence of long-chain fatty acids, which is consistent with the strong surfactant properties characteristic of trehalose lipids. Combining with the chemical evidence from existing studies, these spectral data further validate the structure and properties of the biosurfactant obtained under the optimized conditions.[22]
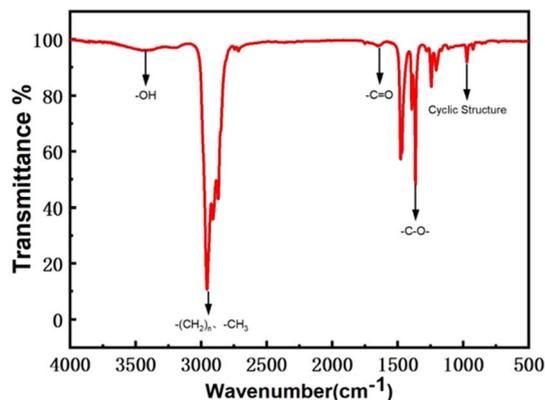
Paper

Fig. 6   The infrared spectrum of the crude product.

3.6.   HPLC-MS analysis

The analysis of high-resolution electrospray ionization mass spectrometry (ESI-MS) in positive ion mode was employed to analyze the structural differences of trehalose lipids produced by *Rhodococcus* sp. WJ-2, both before and after the addition of nano-Fe_2O_3 (SI). In the absence of nano-Fe_2O_3, full-scan mass spectra revealed a series of peaks at m/z 496, 694, 877 and 1044, with integrated signal percentages of 14.19%, 27.08%, 44.18% and 14.55% respectively. These findings suggest that the fatty acid chains of the trehalose lipids were primarily composed of short and medium-chain species, including methyl hexanoate, methyl octanoate, methyl decanoate, methyl tetradecanoate, methyl hexadecanoate, and methyl octadecenoate (Fig. 7, and Table 3). However, after the addition of nano-Fe_2O_3, ESI-MS analysis detected a distinct series of ions at m/z 673, 807, 874

Table 3   Chromatographic results of TLs without Fe_2O_3

Real time	m/z	Positive ion	Proportion
16.425	496	$[M + H]^+$	14.19%
16.425	694	$[M + H]^+$	27.08%
16.668	877	$[M + H]^+$	44.18%
17.417	1044	$[M + H]^+$	14.55%

and 1043, with relative abundances of 22.21%, 18.39%, 47.64% and 11.76% respectively (Fig. 8, and Table 4). Notably, the observed shifts in m/z values and distribution patterns indicate that the trehalose lipids now comprised longer and more hydrophobic fatty acid chains, with an increased propensity for unsaturated fatty acid derivatives. These data collectively demonstrate that minor variations in the length and degree of saturation of fatty acid chains are quite common among the biosurfactant homologs.[10]

Comparing our research findings with the published literature on glycolipid biosurfactants, the results show that the MS data are highly consistent with the previously reported trehalose lipid profiles from *Rhodococcus* species.[16,17] However, our results extend the current understanding by demonstrating that the fermentation conditions, especially the supplementation with iron oxide nanoparticles, can subtly modulate the structural distribution of trehalose lipids. The detected differences in the relative intensities of ions associated with different chain lengths and degrees of unsaturation suggest that nanoparticle-assisted fermentation may have influenced the activities of key enzymes involved in lipid modification. Such modulation could lead to the production of glycolipids with tailored physico-chemical properties, ultimately impacting their emulsification
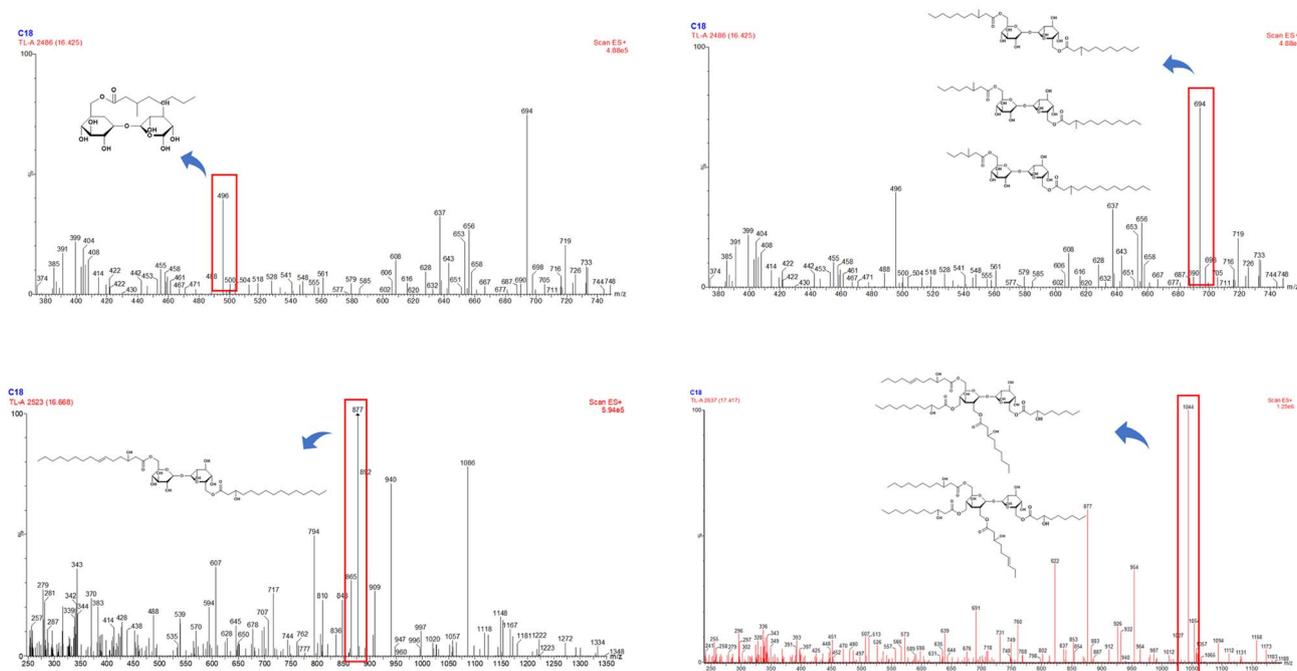
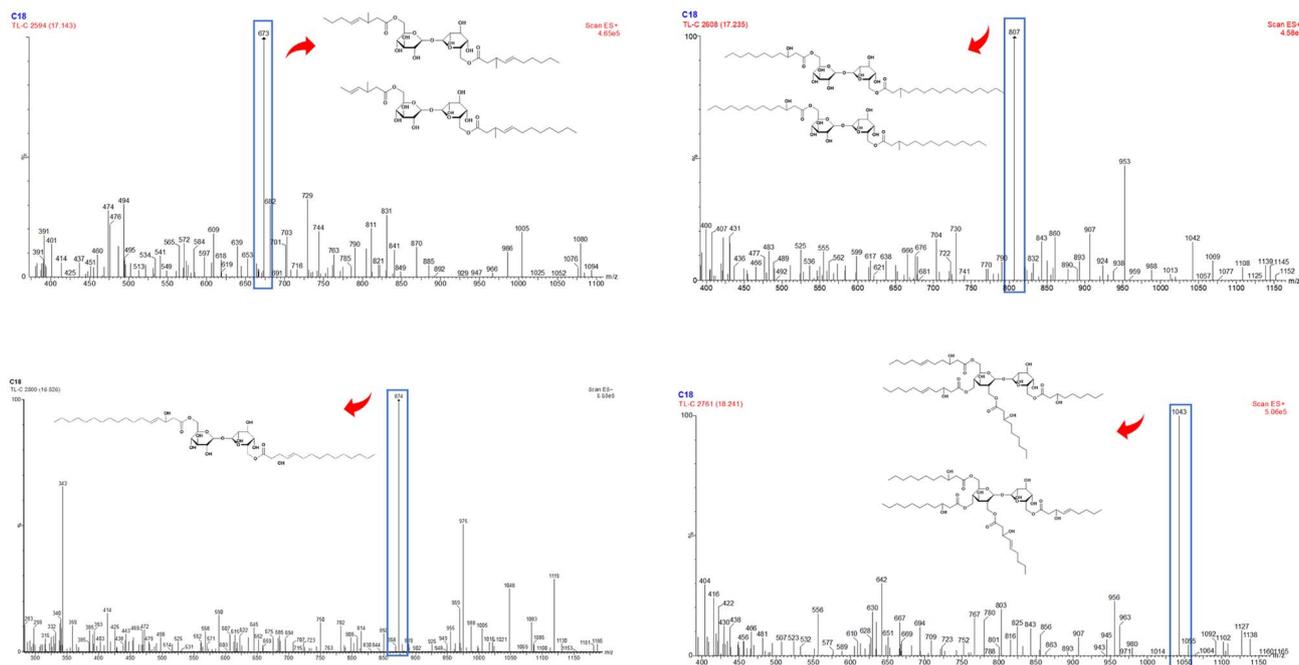Fig. 7   Mass spectrum and structures of trehalose lipids without Fe_2O_3 supplement.

Fig. 8 Mass spectrum and structures of trehalose lipids with Fe_2O_3 supplement.

Table 4 Chromatographic results of TLs with Fe_2O_3

Real time	m/z	Positive ion	Proportion
17.143	673	$[M + H]^+$	22.21%
17.235	807	$[M + H]^+$	18.39%
16.526	874	$[M + H]^+$	47.64%
18.241	1043	$[M + H]^+$	11.76%

the hypothesis that nanoparticles influence cellular metabolism through direct interfacial contact. We hypothesize that nanoparticle surface attachment may locally alter membrane permeability, promoting iron ion transfer and thereby regulating the activity of membrane-bound enzymes in the trehalose lipid synthesis pathway.
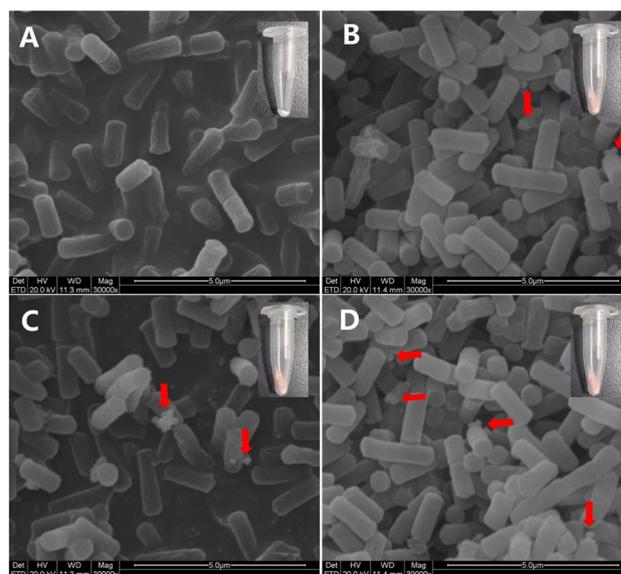
efficiency, CMC, and biological functions.[3,13] The discovery of multiple homologs, each defined by distinct fatty acid chain profiles and glycosidic configurations, highlights the sophisticated biosynthetic abilities of *R. erythropolis* WJ-2. These results enhance our understanding of the structure–function relationships of trehalose lipids and emphasize the potential of nanoparticle-assisted fermentation to optimize biosurfactant production for various industrial applications.

3.7. SEM analysis

Scanning Electron Microscopy (SEM) analysis of bacteria and nanoparticles serves as a powerful tool for understanding the microstructural characteristics of these materials. Therefore, we determined the surface morphology and microstructure of bacteria and bacterial–nanoparticle conjugates through SEM analysis (Fig. 9A–D). *Rhodococcus erythropolis* WJ-2 cells untreated with nanoparticles exhibited smooth surfaces and a typical short rod-shaped morphology (Fig. 9A). In contrast, nanoparticle-treated cells displayed nanoparticles attached to their surfaces (Fig. 9B–D).This close spatial association suggests that electrostatic adsorption or hydrophobic interactions may exist between Fe_2O_3 NPs and the bacterial surface. The morphological characteristics of the complex further support

Fig. 9 SEM of cell and nanoparticle. (A) WJ-2; (B–D) Fe_2O_3 nanoparticles and cell samples obtained at difference culturing time ((B): 2nd day, (C): 5th day, (D): at 7th day; the red arrow points to the NPs. Magnification 30 000×).
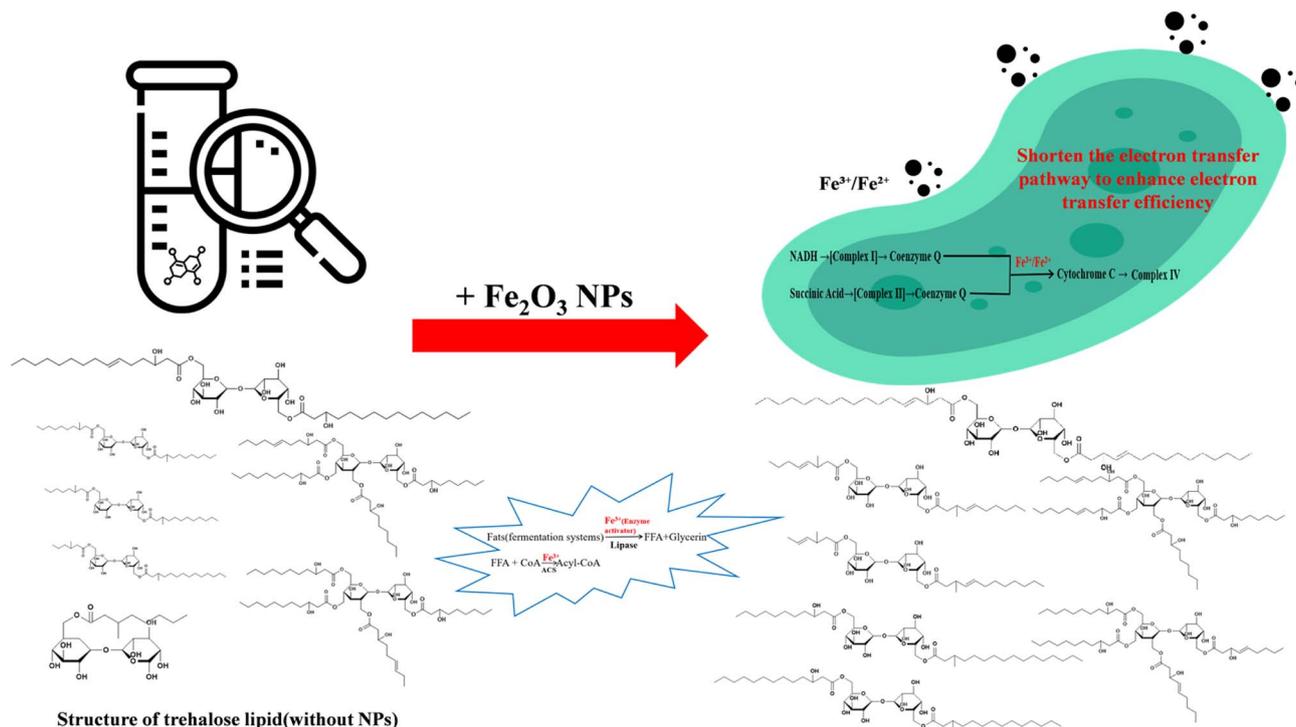
Fig. 10 Mechanism of action of Fe$_2$O$_3$ NPs.

This study hypothesizes that Fe$_2$O$_3$ NPs regulates microbial trehalose lipid biosynthesis through dual metabolic pathways, simultaneously enhancing yield while driving fatty acid side-chain elongation and increased unsaturation (Fig. 10). Fe$_2$O$_3$ NPs interacts with microbial cell membranes, releasing Fe^{3+} into the cytoplasm which act as activators for key enzymes. These enzymes catalyze the hydrolysis of triglycerides into free fatty acids (FFAs) and activate FFAs into acyl-CoA, thereby expanding the fatty acid precursor supply. This enhances the catalytic activity of fatty acid elongase and desaturase, overcoming substrate limitations on chain length and unsaturation. Simultaneously, Fe$_2$O$_3$ NPs leverages its Fe^{3+}/Fe^{2+} redox cycling capacity as an exogenous electron shuttle. This shortens electron transfer pathways, maintains redox homeostasis to mitigate reactive oxygen species (ROS)-induced damage to the electron transport chain (ETC), and enhances ATP and NADPH supply. Consequently, both the chain length and activity of the final product are further elevated.

4. Conclusion

This study demonstrates the dual benefits of integrating iron oxide nanoparticles into the fermentation process of *Rhodococcus erythropolis* WJ-2 for trehalose lipid production. By first establishing sunflower oil as the superior carbon source and then optimizing medium components through a Box–Behnken design, we achieved a baseline yield of approximately 24.75 g L^{-1}. The targeted addition of 0.5 g per L Fe$_2$O$_3$ nanoparticles further enhanced production by around 10% and was found to subtly modulate the molecular architecture of the produced

glycolipids, as confirmed by FTIR and high-resolution HPLC-MS analyses. These structural modifications, characterized by shifts in functional group vibrations and changes in fatty acid chain lengths and degrees of saturation, indicate that nanoparticle-mediated effects can alter enzyme kinetics and metabolic pathways during lipid assembly. These findings support the promise of nanoparticle-assisted fermentation as a strategy for producing tailored, high-performance biosurfactants for diverse industrial applications.

The addition of iron oxide nanoparticles significantly increased the yield of trehalose lipids, which is consistent with previous studies demonstrating the promoting effects of nanoparticles on microbial metabolism. For example, iron oxide nanoparticles could enhance cellular metabolic activity by modulating the redox state and electron transport chain of microorganisms, thereby improving the synthesis efficiency of target products.[28] Similarly, the nanoparticles could optimize the flux distribution of metabolic pathways by influencing the availability of enzyme cofactors, such as iron ions.[29] Our study further supports this notion, as the addition of Fe$_2$O$_3$ NPs likely enhanced the activity of enzymes involved in lipid synthesis, such as glycosyltransferases and fatty acid synthases, by providing iron ions as cofactors.

Through FTIR and HPLC-MS analyses, we found that the addition of Fe$_2$O$_3$ NPs led to changes in the molecular structure of glycolipids, including shifts in functional group vibrations and alterations in fatty acid chain length and degree of saturation. These results align with the findings of Rodrigues *et al.*,[30] who highlighted that the molecular structure of biosurfactants significantly influences their properties, such as emulsification

and stability. Additionally, Marchant and Banat[31] demonstrated that the length and saturation of fatty acid chains directly affect the surface activity of glycolipids, with longer chains and higher degrees of unsaturation typically associated with better emulsification performance. Our results suggest that Fe_2O_3 NPs may optimize the molecular structure of glycolipids by modulating enzyme kinetics in the lipid synthesis pathway, thereby enhancing their performance.

Similar to our study, nanoparticles have been widely applied in microbial fermentation, including enhancing product yield and optimizing product performance. However, compared to precious metal nanoparticles such as gold and silver, iron oxide nanoparticles offer advantages such as lower cost and higher biocompatibility, making them more suitable for large-scale industrial applications. Additionally, Gopalakrishnan, K. et al.[32] reported that nanoparticle-assisted fermentation technology is not only applicable to glycolipid production but can also be extended to the biosynthesis of other high-value compounds, such as biohydrogen. Our study further validates the potential of this technology and provides new evidence for its application in biosurfactant production, which advance the field of nanoparticle-assisted biosurfactant synthesis. Previous studies on nanoparticle-mediated lipid biosynthesis have primarily focused on other classes of biosurfactants (e.g., rhamnolipids and sophorolipids) or different microbial hosts, leaving the specific regulatory mechanisms governing trehalose lipid biosynthesis largely unexplored. This study addresses this research gap by investigating the specific interaction between Fe_2O_3 NPs and *Rhodococcus erythropolis* WJ-2 for trehalose lipid production. Moreover, by integrating FTIR and HPLC-MS analyses, we elucidate the mechanistic role of nanoparticles, linking Fe_2O_3 NP-induced modulation of enzyme kinetics to specific structural alterations. This approach provides mechanistic insights that advance beyond the primarily descriptive nature of earlier research on nanoparticle-assisted fermentation. A systematic comparison with other nanoparticle systems used in lipid biosynthesis further highlights the novelty and superiority of Fe_2O_3 NPs in this study. Precious metal nanoparticles have shown comparable yield-promoting effects by enhancing membrane permeability and enzyme activity, but their exorbitant cost, poor biocompatibility at high concentrations, and potential environmental persistence render them unfeasible for large-scale industrial application. ZnO NPs act as cofactors for acetyl-CoA carboxylase, only modulate lipid yield without significant structural regulation of the end product, limiting their ability to tailor biosurfactant performance. In contrast, Fe_2O_3 NPs offer a balanced combination of cost-effectiveness, high biocompatibility with *R. erythropolis*, and dual functional roles, enabling simultaneous yield improvement and structural optimization of trehalose lipids. This unique set of advantages positions Fe_2O_3 NPs as a more practical and versatile tool for industrial-scale biosurfactant production compared to other nanoparticle systems.

Nanoparticle-assisted fermentation technology not only improves product yield but also optimizes product performance through the modulation of molecular structures, thereby offering significant potential for industrial applications. For instance, Sekhon Randhawa and Rahman[33] emphasized the substantial application value of biosurfactants in various fields, including petroleum extraction, environmental remediation, and pharmaceuticals. Our study demonstrates that nanoparticle-assisted fermentation enables the production of glycolipids with tailored properties, such as enhanced emulsification capacity and antimicrobial activity, to address diverse industrial requirements. This structural customization capability paves the way for developing novel functional materials. For instance, by precisely controlling the hydrophobic chain length and unsaturation degree of trehalose lipids, surfactants with specific critical micelle concentration (CMC) and interfacial ordering behavior can be designed for constructing smart emulsification systems or responsive materials. Furthermore, trehalose lipids regulated by nanoparticle-assisted methods, which can serve as green templates for synthesizing mesoporous materials due to their unique molecular structure. They demonstrate application potential in chemical and materials fields such as catalysis, sensing, and drug delivery. Furthermore, in contrast to chemically synthesized surfactants, biosurfactants exhibit superior environmental compatibility and biodegradability, which aligns with the principles of sustainable development.

Although our study has achieved positive results, the mechanisms underlying the interactions between nanoparticles and microorganisms still require further exploration. Building on these findings, the present work opens up promising future research directions in the field of nanoparticle-assisted biosurfactant synthesis. By integrating multi-omics technologies (transcriptomics, proteomics, and metabolomics), we can elucidate the global regulatory network of *Rhodococcus erythropolis* WJ-2 in response to Fe_2O_3 nanoparticles, thereby identifying key genes, proteins, and metabolic intermediates involved in trehalose lipid structural modification, which will fill critical gaps in the current understanding of nanoparticle-microbe metabolic crosstalk. Additionally, future research could investigate the impact of different types and concentrations of nanoparticles on the fermentation process to further optimize product yield and performance. Moreover, this strategy can be extended to other microbial strains or mixed consortia capable of producing trehalose lipids, to investigate whether the regulatory effects of Fe_2O_3 nanoparticles are conserved or strain specific. This exploration will help broaden the applicability of this technology. Furthermore, pilot-scale validation of Fe_2O_3 nanoparticle-assisted production should be conducted to evaluate key parameters such as nanoparticle recyclability, process cost and product quality stability, thereby providing a robust foundation for translating laboratory research into industrial applications.

Author contributions

Yifei Meng: writing – review & editing, investigation, data curation, validation. Xuan Ou: investigation, data curation, methodology; Zhenghui Liu: validation, data curation; Shun Yao: data curation; Chuxiao Hu: data curation; QiuchiYu: sampling; Wenjie Xia: conceptualization, investigation, writing

Conflicts of interest

The authors declare that they have no conflict of interests.

Data availability

Other data that support the findings of this study are available from the corresponding author upon reasonable request.

Supplementary information (SI) is available. See DOI: https://doi.org/10.1039/d5ra09253a.

Acknowledgements

References

1 K. Gautam, P. Sharma, V. K. Gaur, P. Gupta, U. Pandey and S. Varjani, *Environ. Technol. Innov.*, 2023, **30**, 103095.

2 S. Sánchez Muñoz, T. R. Balbino, E. Mier Alba, F. G. Barbosa, F. T. de Pier and A. L. Moura de Almeida, *Bioresour. Technol.*, 2022, **345**, 126477.

3 T. Ingsel, F. M. de Souza and R. K. Gupta, *Green Sustainable Process Chem. Environ. Eng. Sci.*, 2022, 467–493.

4 D. Gao, H. Zhao, L. Wang, Y. Li, T. Tang and Y. Bai, *J. Environ. Manage.*, 2022, **320**, 115799.

5 E. Eras-Muñoz, A. Farré, A. Sánchez, X. Font and T. Gea, *Bioengineered*, 2022, **13**(5), 12365–12391.

6 S. Naidu, I. K. Singh and A. Singh, *Plant Nano Biol.*, 2023, **4**, 100036.

7 R. Kumar, R. I. Barbhuiya, V. Bohra, J. W. C. Wong, A. Singh and G. Kaur, *Microbiol. Res.*, 2023, **272**, 127386.

8 A. R. Markande, D. Patel and S. Varjani, *Bioresour. Technol.*, 2021, **330**, 124963.

9 S. K. Satpute, A. G. Banpurkar, P. K. Dhakephalkar, I. M. Banat and B. A. Chopade, *Crit. Rev. Biotechnol.*, 2010, **30**(2), 127–144.

10 S. Lopes, E. Fahr and J. Costa, *Bioprocess Biosyst. Eng.*, 2024, **47**, 145–157.

11 S. A. Qamar and S. Pacifico, *J. Environ. Chem. Eng.*, 2023, **11**(6), 111555.

12 J. D. Liu, X. M. Hu, Y. Feng, Y. Y. Zhao, M. Y. Wu and X. W. Wang, *J. Environ. Chem. Eng.*, 2022, **10**(3), 107764.

13 J. Yu, R. Xie and J. Yu, *J. Soils Sediments*, 2023, **23**, 1745–1759.

14 W. R. Finnerty, *Curr. Opin. Biotechnol.*, 1994, **5**(3), 291–295.

15 Q. Zhang, J. Teng, R. Zhou and L. Mai, *J. Hubei Univ.*, 2009, **31**(1), 68–70.

16 A. Alvarez, B. Rodríguez-Garrido, A. Cerdeira-Pérez, A. Tomé-Pérez, P. Kidd and A. Prieto-Fernández, *J. Hazard Mater.*, 2022, **433**, 128764.

17 M. Yu, Z. Zhu, B. Chen, Y. Cao and B. Zhang, *Front. Microbiol.*, 2022, **13**, 860458.

18 M. Pacwa-Płociniczak, G. A. Płaza, Z. Piotrowska-Seget and S. S. Cameotra, *Int. J. Mol. Sci.*, 2011, **12**(1), 633–654.

19 Y. M. Yuan, X. H. Xing and C. Zhang, *Synth. Biol. J.*, 2020, **1**(6), 656–673.

20 N. Xu, Y. Liu, H. Jiang, J. Liu and Y. Ma, *Curr. Opin. Biotechnol.*, 2020, **66**, 27–35.

21 W. J. Holtz and J. D. Keasling, *Cell*, 2010, **140**(1), 19–23.

22 R. K. Sharma, G. Dey, P. Banerjee, J. P. Maity, C. M. Lu and J. A. Siddique, *J. Mater. Chem. B*, 2022, **11**(1), 10–32.

23 M. Rai, A. Yadav and A. Gade, *Biotechnol. Adv.*, 2009, **27**(1), 76–83.

24 M. J. Hajipour, K. M. Fromm, A. A. Ashkarran, D. J. de Aberasturi, I. Ruiz de Larramendi and T. Rojo, *Trends Biotechnol.*, 2012, **30**(10), 499–511.

25 P. Rananaware, S. Bauri, R. Keri, M. Mishra and V. Brahmkhatri, *Environ. Sci. Pollut. Res.*, 2024, **31**, 46625–46640.

26 A. Nel, L. Mädler and D. Velegol, *Nat. Mater.*, 2009, **8**, 543–557.

27 J. Ji, L. Li, W. Guo, J. Zhang, Y. Yao and H. Chen, *Fundam. Res.*, 2025, **5**(5), 1889–1910.

28 B. Koul, A. K. Poonia, D. Yadav and J. O. Jin, *Biomolecules*, 2021, **11**(6), 886.

29 C. Zhu, J. Zhou, Y. Wang and Y. Wang, *Curr. Opin. Biotechnol.*, 2020, **64**, 161–168.

30 L. R. Rodrigues, J. A. Teixeira, H. C. van der Mei and R. Oliveira, *Colloids Surf., B*, 2006, **49**(1), 79–86.

31 R. Marchant and I. M. Banat, *Biotechnol. Lett.*, 2012, **34**(9), 1597–1605.

32 K. Gopalakrishnan, T. Mathimani, E. R. Rene and A. Pugazhendhi, *Int. J. Hydrogen Energy*, 2019, **44**(26), 13106–13113.

33 P. K. Rahman and K. K. Sekhon Randhawa, *Front. Microbiol.*, 2014, **5**, 454.